Environmental Science & Technology

Article

Cite This: Environ. Sci. Technol. 2018, 52, 7680−7688

pubs.acs.org/est

Particle-Phase Photosensitized Radical Production and Aerosol Aging

Pablo Corral Arroyo,[†,‡] Thorsten Bartels-Rausch,[†] Peter A. Alpert,[†] Stéphane Dumas,[§] Sébastien Perrier,[§] Christian George,[§] and Markus Ammann*[,†]

[†]Paul Scherrer Institute, Laboratory of Environmental Chemistry, 5232 Villigen PSI, Switzerland

[‡]Department of Chemistry and Biochemistry, University of Bern, 2012 Bern, Switzerland

[§]CNRS, UMR5256, IRCELYON, Univ. Lyon, Université Claude Bernard Lyon 1, CNRS, IRCELYON, F-69626, Villeurbanne, France

Supporting Information

ABSTRACT: Atmospheric aerosol particles may contain light absorbing (brown carbon, BrC), triplet forming organic compounds that can sustain catalytic radical reactions and thus contribute to oxidative aerosol aging. We quantify UVA induced radical production initiated by imidazole-2-carboxaldehyde (IC), benzophenone (BPh). and 4-benzoylbenzoic acid (BBA) in the presence of the nonabsorbing organics citric acid (CA), shikimic acid (SA), and syringol (Syr) at varying mixing ratios. We observed a maximum HO_2 release of 10^{13} molecules min^{-1} cm^{-2} at a mole ratio $X_{BPh} < 0.02$ for BPh in CA. Mixtures of either IC or BBA with CA resulted in 10^{11}−10^{12} molecules min^{-1} cm^{-2} of HO_2 at mole ratios (X_{IC} and X_{BBA}) between 0.01 and 0.15. HO_2 release was affected by relative humidity (*RH*) and film thickness suggesting coupled photochemical reaction and diffusion processes. Quantum yields of HO_2 formed per absorbed photon for IC, BBA and BPh were between 10^{-7} and 5×10^{-5}. The nonphotoactive organics, Syr and SA, increased HO_2 production due to the reaction with the triplet excited species ensuing ketyl radical production. Rate coefficients of the triplet of IC with Syr and SA measured by laser flash photolysis experiments were $k_{Syr} = (9.4 \pm 0.3) \times 10^8$ M^{-1} s^{-1} and $k_{SA} = (2.7 \pm 0.5) \times 10^7$ M^{-1} s^{-1}. A simple kinetic model was used to assess total HO_2 and organic radical production in the condensed phase and to upscale to ambient aerosol, indicating that BrC induced radical production may amount to an upper limit of 20 and 200 M day^{-1} of HO_2 and organic radical respectively, which is greater or in the same order of magnitude as the internal radical production from other processes, previously estimated to be around 15 M per day.

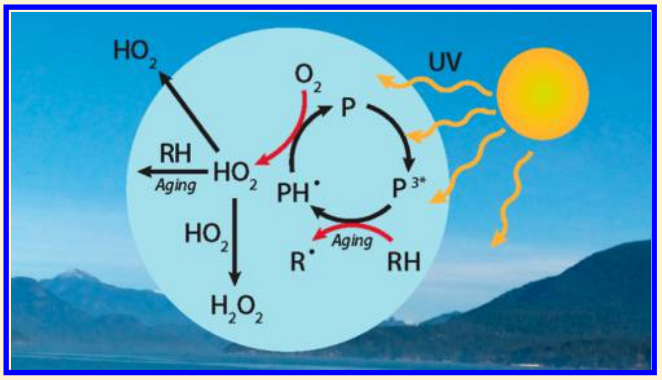

INTRODUCTION

Brown carbon (BrC), defined as the fraction of organic compounds in atmospheric aerosol particles that absorb efficiently in the UVA-VIS range, is ubiquitously present in the troposphere.[1−3] Absorption of solar radiation by BrC has been estimated at 0.1−0.25 W m^{-2} globally, which is approximately 25% of the radiative forcing by black carbon or soot.[3] Photochemistry initiated by BrC species can change their own chemical composition and both enhance and decrease light absorption over time.[4,5] These processes may be related to triplet forming BrC species, so-called photosensitizers, which may catalyze radical chain reactions. Photosensitized chemistry is well-established in aquatic photochemistry[6] and has been recently recognized as contributors to the oxidant budget in airborne particles.[7−9] This may therefore represent an important contribution to aerosol aging, which refers to the chemical transformations induced by uptake of gas phase radicals such as OH, HO_2 or NO_3,[7,10,11] to cloud droplets or particles,[12] by partitioning of low volatility compounds following the oxidation of the precursors in the gas phase, and by condensed phase chemical processes. Recently, HO_2 release in organic mixtures with imidazole-2-carboxaldehyde (IC) as photosensitizer and citric acid (CA) was determined as a function of relative humidity (*RH*) and IC concentration.[8] Here, we expand to another photosensitizer family and measure photosensitized HO_2 release for IC, benzophenone (BPh) and 4-Benzoylbenzoic acid (BBA). In addition, we quantify the influence of different nonabsorbing compounds, shikimic acid (SA) and syringol (Syr) on the IC initiated HO_2 release. Finally, we elucidate chemical cycling using a simple steady-state kinetic model to infer the internal HO_2 and organic radical production. We evaluate the relative importance of internal photochemical

Received: January 18, 2018
Revised: May 29, 2018
Accepted: June 13, 2018
Published: June 13, 2018

DOI: 10.1021/acs.est.8b00329
Environ. Sci. Technol. 2018, 52, 7680−7688

radical production in comparison to oxidant uptake from the gas phase and other internal sources.

Many known photosensitizers are carbonyls, which absorb above 300 nm especially when the carbonyl function is attached to an aromatic system. Figure 1 illustrates the catalytic

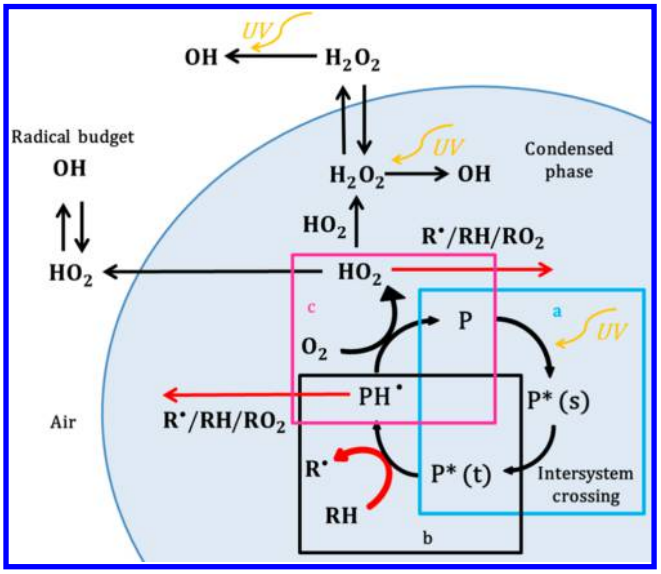

Figure 1. Photochemical catalytic cycle of a photosensitizer (P) in a particle. (a) P first absorbs light being excited to the triplet state (P*(t)). (b) The triplet reacts with an H atom/electron donor to produce the reduced ketyl radical (PH•). (c) The ketyl radical may transfer an H atom or electron to an acceptor, such as O_2. HO_2 radicals can then be released into the gas phase or react within the particle. Red reaction arrows indicate aging reactions of condensed phase organic molecules. Acid dissociation of HO_2 is not shown for simplicity.

cycle of a photosensitizer (P) with an initial excitation step indicated by the blue box (box a), followed by singlet (P*(s)) to triplet (P*(t)) intersystem crossing (ISC). P*(t) state is long-lived and can act as an oxidant[6] toward any organic compound (the "donor", RH), in the present study represented by CA, SA, and Syr. This leads to an alkyl or phenoxy radical and a ketyl radical (PH•) as illustrated in the black box b in Figure 1. PH• passes on an electron or hydrogen atom to oxygen or another electron acceptor (e.g., NO_2)[13] illustrated in the magenta box c in Figure 1 and leads back to P in its ground state. The efficiency of the catalytic cycle is reduced by several processes involving P*(s) and P*(t) such as deactivation of P*(s), deactivation of P*(t), that is, by phosphorescence, nonradiative decay, and reaction with oxygen. Radical reactions of PH• also influence the efficiency of the catalytic cycle. Overall, formation of P*(t) leads to the oxidation of RH and to the production of HO_2. Therefore, this indirect photochemistry may drive oxidation under those daytime tropospheric conditions that are characterized by low flux at wavelengths below 300 nm, where direct photolysis of the majority of organic compounds is not possible and HO_x production in the gas phase is not efficient.

Imidazoles, which include IC, are BrC compounds formed as products from the multiphase chemistry of glyoxal and ammonium sulfate (AS) in aqueous aerosols.[9,14,15] Glyoxal is an important oxygenated volatile organic compound (OVOC) originating from the oxidation of predominantly biogenic precursors. BPh, BBA,[6] and other aromatic carbonyls may be formed as intermediates in the photooxidation of aromatic compounds in the gas phase[16,17] or also by condensed phase oxidation of biomass burning products.[18,19] CA serves as a proxy for nonabsorbing, highly oxidized and functionalized secondary organic compounds in the atmosphere. In solution, CA takes up or releases water gradually without phase change over the whole range of relative humidity (*RH*) values studied here,[20,21] which makes it a good substrate and matrix from an experimental perspective. SA is considered a proxy for reactive oxygenated organic material and has been found in biomass burning aerosol.[22] It is condensed phase ozonolysis kinetics has been investigated previously.[23−25] Syr is a well-known thermal decomposition product of lignin occurring in biomass burning aerosol from hard woods[26,27] and known to act as a single-electron reductant with NO_2 and other oxidants.[28,29]

EXPERIMENTAL SECTION

Coated-Wall Flow Tube Experiments. The HO_2 release was measured by scavenging HO_2 with an excess of nitrogen monoxide (NO) in an irradiated reactor containing a laminar coated wall flow tube (CWFT). The method has been described in detail in our previous work[8] and further details, raw data from exemplary experiments and the rationale of the conversion of the measured NO loss to HO_2 release rate are given in the SI. The coated tubes were 1.2 cm inner diameter, 50 cm long (Duran glass) and fitted snuggly into the reactor as inserts. The jacketed glass reactor held at $T = 20 \pm 1$ °C was surrounded by 7 fluorescent lamps (UVA range, Philips Cleo Effect 20W = 300−420 nm, 41 cm, 2.6 cm o.d., see Figure S1), leading to J_{NO_2} of 0.011 s^{-1} in the flow tube. Flows of N_2 and O_2 were set by mass flow controllers at 1 L/min and 0.5 L/min, respectively. NO was added with a third flow of 5−10 mL/min of 100 ppm of NO in N_2. The NO concentration during CWFT experiments was always in excess of 10^{13} molecules cm^{-3} to efficiently scavenge 99% of HO_2 produced by the films within at most 50 ms ($k_1 = 8.0 \times 10^{-12}$ cm^3 $molecule^{-1}$ s^{-1} at 298 K:[30] $t_{99\%} = \frac{-\ln(0.01)}{k_1[NO]}$). The lifetime of HO_2 with respect to its self-reaction in the gas phase is about 20 s ($[HO_2] = 5$ ppb and $k_{HO_2} = 1.8 \times 10^{-12}$ cm^3 $molecule^{-1}$ s^{-1} at 298 K.[31]

$$NO + HO_2 \rightarrow NO_2 + OH \quad (1)$$

RH from 25 to 65% at 20 °C was controlled using two different humidifier apparatus, in which the carrier gas passed either through a permeable tube immersed in liquid water at $T > 293$ K or over liquid water at $T < 293$ K to a desired dew point. The flow was directed to bypass the reactor to exchange flow tubes without the need to interrupt the flow system and to determine the initial trace gas levels at the entrance of the CWFT. The concentration of NO was measured by a chemiluminescence detector (Ecophysics CLD 77 AM). H_2O_2 was measured by the AeroLaser 2021 analyzer.

The preparation of the films composed of IC and CA and their properties are described in our previous work.[8] The IC/CA, BPh/CA, and BBA/CA films were produced by depositing 400 μL of aqueous solutions of 0.75 M of CA and varying amounts of IC, BPh, or BBA in the glass tube inserted. A homogeneous, thin and viscous film in equilibrium with the same RH as used later in the experiment was achieved by rolling and turning the tube in all directions at room temperature under a gentle flow of humidified N_2. Solutions

DOI: 10.1021/acs.est.8b00329
Environ. Sci. Technol. 2018, 52, 7680−7688

were prepared prior to each experiment and kept in the dark. The thickness of the film after equilibration with the given RH was estimated from the hygroscopic volume growth factors of CA,[21] assuming that the water content was dominated by the properties of CA. Final concentrations in the film were 5 M of CA, 0.1−0.6 M for IC and BBA and 0.02−0.1 M for BPh at 35% RH. For CWFT experiments with SA and Syr the mole ratio IC/(CA+SA) and IC/(CA+Syr) was kept constant at 0.15 at 40% RH, while increasing SA and Syr concentrations. Conditions of CWFT experiments are summarized in Table S1. Blank experiments run with noncoated tubes were routinely performed in between experiments with coated tubes and always resulted in NO losses below detection limit. In order to exclude other sources of HO_2, films composed only of IC were irradiated, which did not result in detectable NO loss. A commercial O_3 analyzer (Photometric O_3 Analyzer − Model 400E; TELEDYNE Instruments) was used to check the absence of O_3 (detection limit 2 ppb).

Aerosol Flow Tube Experiments. An irradiated aerosol flow tube (AFT) experiment was also used in the exact same configuration as the CWFT experiments to measure HO_2 release from IC/CA particles. The AFT is 156 cm long, 7 cm inner diameter and fabricated with Teflon perfluoroalkoxy copolymer (PFA). Lamps for irradiation (UVA range, Philips Cleo Effect 70 W = 300−420 nm, 150.7 cm, 2.8 cm o.d., emission spectrum identical to those of CWFT, Figure S1) resulted in a J_{NO_2} value of 0.011 s^{-1}. Gas flow in the AFT consisted of 0.8 L/min of N_2, 0.2 L/min of O_2, and a third flow of NO/N_2 to maintain the NO concentration at ∼2.5 × 10^{13} molecules cm^{-3}. A particle filter downstream of the AFT was used to prevent particles from entering the NO analyzer. More details on the experimental procedure and exemplary raw data are shown in the SI.

Laser Flash Photolysis Experiments. The decay rate of the excited triplet state of IC in the presence of SA and Syr was measured in aqueous solution by laser flash photolysis (LFP), as described in detail in the SI.

Chemicals. The chemicals used were imidazole-2-carboxaldehyde (>99%, Aldrich), benzophenone (>99%, Aldrich), 4-benzoylbenzoic acid (>99%, Aldrich), citric acid (Fluka), shikimic acid (Alfa Aesar, 98%), and 2,6-dimethoxyphenol (99%, Aldrich). The water used was Milli-Q water (18mΩ).

RESULTS

Influence of Photosensitizer Type and Mixing Ratio. Figure 2 presents the HO_2 radical release in the CWFT as a function of the photosensitizer/CA mole ratio at constant CA mass (76.8 mg) at a RH of 43−47% for IC and 53−57% for BPh and BBA. The largest HO_2 release of 10^{13} molecules cm^{-2} min^{-1} was due to the BPh/CA mixture at a X_{BPh} of 0.025 and decreased to 1.6 × 10^{12} molecules cm^{-2} min^{-1} at a X_{BPh} of 0.002. The HO_2 release for the mixture of BBA/CA was (0.2−0.7) × 10^{12} molecules cm^{-2} min^{-1}, while for the mixture of IC/CA the release amounted to (0.1−0.3) × 10^{12} molecules cm^{-2} min^{-1} for mole ratios (X_{BBA} and X_{IC}) between 0.02 and 0.08 and 0.03−0.13, respectively. Despite BPh having the lowest absolute concentration, it resulted in the greatest HO_2 release reflecting its larger absorbance at wavelengths >320 nm (Figure S1) and more efficient radical production.

The measurements of the HO_2 release as a function of film thickness (Figure S7)[8] exhibits an increase until around 3 μm and then tends to level off or decrease until 5.5 μm. This indicates that (i) the primary excitation is occurring predominantly throughout the bulk of the film and that (ii) the observed HO_2 release is contributed from the upper 3 μm. The fact that the roughly linear initial increase of HO_2 with film thickness exhibits a small offset may indicate a surface contribution, as discussed below. These results are consistent with the AFT measurements shown in Figure S8, where we observed 2 orders of magnitude more HO_2 release per unit mass likely due to the shorter depth, from which HO_2 molecules leave the condensed phase.

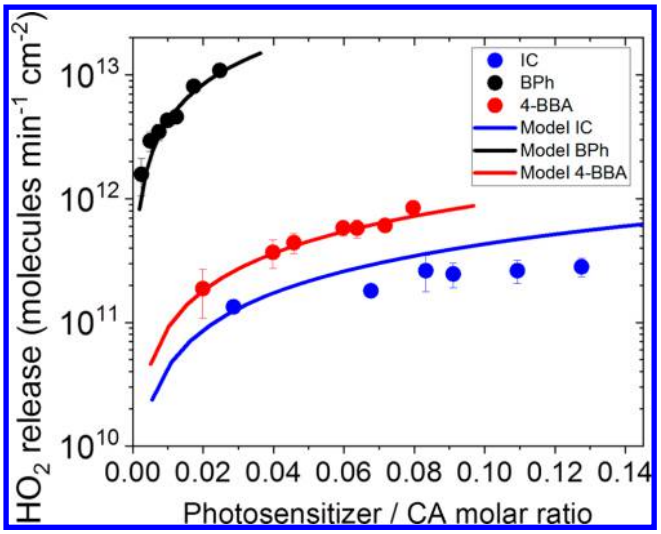

Figure 2. Measured HO_2 radical release as a function of the ratio of photosensitizer to citric acid (CA) for BPh at 45% RH, 4-BBA at 45% RH, and IC at 55% RH (black, red, and blue symbols, respectively). Error bars are determined from the standard deviation of several replicate measurements. Solid lines are fits using the model described in the text.

The absence of O_3 and the fact that the amount of HONO formed was nearly half of the NO loss (see SI) is a strong indication that HO_2 was actually the dominant oxidant. Photolysis of HONO was too slow (J_{HONO} = 0.0024 s^{-1}) to initiate additional gas phase radical chemistry. Measurements were done over 100 h of irradiation for IC/CA without any significant drop of the HO_2 release, which confirms the photocatalytic nature of the process. We cannot entirely exclude secondary chemistry of the oxidized donor that may lead to elimination of HO_2 and thus contribute to NO loss.

Influence of Relative Humidity. Figure 3 shows the HO_2 release at constant dry masses of CA and constant mole ratio of photosensitizers as a function of RH (Figure 3a). As RH increases from about 40%, HO_2 release decreases by about 1 order of magnitude for IC, BBA and BPh. However, the trends of HO_2 release are dissimilar among the three below 40% *RH*. For IC/CA and RH increasing from 0 to 20% the HO_2 release increases to a plateau of 2 × 10^{11} molecules cm^{-2} min^{-1} at RH between 20 and 40%. In contrast, for BBA/CA and BPh/CA, HO_2 fluxes are much higher for dry conditions and then decrease toward 40% RH.

Quantum yields of observed HO_2 release per absorbed photon for these experiments calculated based on absorption and lamp emission spectra (Figure S1) are shown in Figure 3b. In the high RH region, the quantum yield is highest for IC and lowest for BBA, possibly caused by a lower ISC yield, faster deactivation of P*(t), additional sinks for $PH^{\bullet}$,[33] lower rate of

DOI: 10.1021/acs.est.8b00329
Environ. Sci. Technol. 2018, 52, 7680−7688

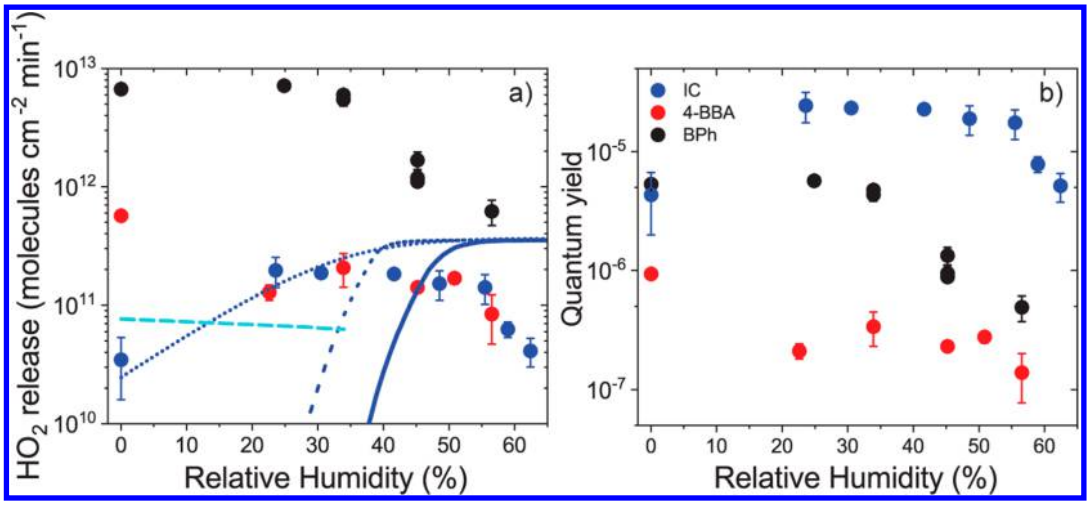

Figure 3. (a) Measured HO_2 release (symbols) as a function of *RH* at a fixed mole ratio of photosensitizer to CA (0.08 for BPh, 0.08 for 4-BBA, 0.11 for IC). Blue lines show model calculations for the case of IC based on the parametrization of the diffusion coefficient by Lienhard et al.,[32] with and without an assumed water activity dependence of the rate coefficient for the HO_2 self-reaction (dashed and solid line, respectively). The blue dotted line represents the model prediction with adjusted diffusivity. The dashed purple line represents a suspected surface reaction. See text for more details. (b) Quantum yield HO_2 release of versus RH for the same experiments. Error bars are determined from the standard deviation of several replicate measurements.

the reaction between P*(t) and CA or competing processes, such as secondary chemistry of HO_2.

The observed RH dependence (Figure 3a) may be qualitatively understood in the context of RH driven water activity to dilute or concentrate the reactants, to affect the viscosity and thus molecular diffusion, and likely by phase separation occurring at low RH. At RH between 40% and 60%, where the mixtures with CA are presumably homogeneous solutions, water activity increases, which we expected to control the decrease of the HO_2 production for all three photosensitizers due to the decreasing concentrations of donor, triplets, and radical intermediates caused by the dilution by water. At low RH (low water activity) little change in volume and thus donor concentration occurs, but the viscosity of the films increases,[34] which we expected to lead to decreasing HO_2 production and release because of low diffusivity of all involved species. The complex interplay of these effects will be examined together with the kinetic model in the Discussion section.

When different types of organic matter (BBA and BPh mixed with CA) are present in aqueous solution, they may phase separate, which we hypothesize to occur for BBA and BPh between 0%−20% RH and 35−40% RH, respectively, due to differences in polarity and solubility, similar to cases of organic solutes mixed with inorganic salts.[35−37] Phase separation may lead to an accumulation of the more surface active photosensitizers at the film−air interface increasing its local concentration there and thus increasing reaction rates of P*(t) or $PH^{\bullet}$ and thereby also the HO_2 release into the gas phase. Due to this complication, we only consider the IC-CA system in our further more quantitative discussion of the behavior under dry conditions.

Influence of Competing Donors. Figure 4 shows the HO_2 release for the two systems IC/Syr/CA and IC/SA/CA as a function of the Syr or SA donor concentration. Experiments employed constant IC and CA concentration at 0.7 and 6 M, respectively. For comparison, observed HO_2 release for the IC/CA system without any additional donor is shown as the blue line in Figure 4. At a concentration around 10^{-4} M for Syr

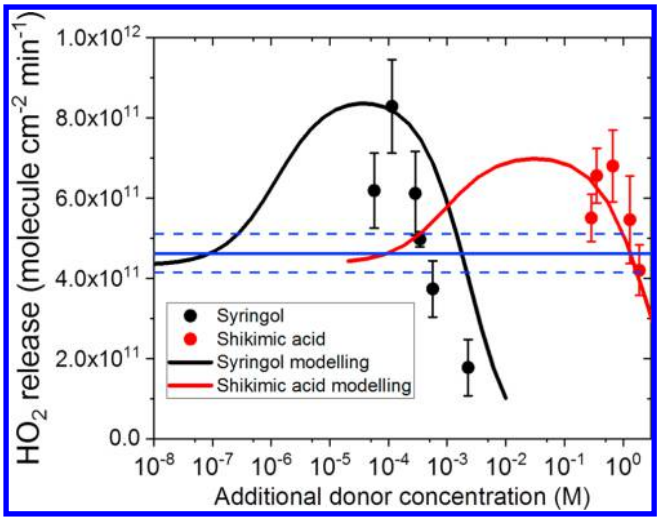

Figure 4. HO_2 radical release photosensitized by IC in the presence of citric acid and Syr (black squares) and SA (red circles) as additional competing donors, respectively, both at constant IC (0.7 M) and CA (6 M) load at 45% RH. Error bars are determined from the standard deviation of several replicate measurements. Black and red lines represent the HO_2 release returned by the kinetic model described in the text for Syr and SA, respectively. The blue line and dashed lines indicate the measured HO_2 release and the error range, respectively, in absence of any additional donor apart from CA.

and 0.5 M for SA, HO_2 release was enhanced compared to experiments using IC/CA. In turn, HO_2 release decreases by about a factor of 5 as the donor concentration increases further by a factor of about 50.

The enhancement of the HO_2 release at low additional donor concentration may result from increased $PH^{\bullet}$ production, that is, the additional donors compete with CA for oxidation by P*(t). The concentration at which Syr and SA provide faster $PH^{\bullet}$ production is related to the ratio between the rate coefficient of the P*(t) with CA and that of the IC triplet with either of the additional donors. These rate coefficients were measured by laser flash photolysis (LFP) as

DOI: 10.1021/acs.est.8b00329
Environ. Sci. Technol. 2018, 52, 7680−7688

shown in Figure S6: $k_{SA} = (2.7 \pm 0.5) \times 10^7$ M^{-1} s^{-1} for SA (pH = 7) and $k_{Syr} = (9.4 \pm 0.3) \times 10^8$ M^{-1} s^{-1} for Syr (pH = 6.5). The rate coefficient of the reaction between the P*(t)and CA, $k_{IC/CA}$, was below the detection limit of 10^5 M^{-1} s^{-1}. We note that k_{Syr} is about 36 times greater than k_{SA}. Though, the concentration ranges of Syr and SA, at which enhanced HO_2 and its drop was observed, differ by a factor of 1000, implying that additional chemical reactions, such as those of $PH^{\bullet}$ and HO_2 with the donors or their oxidation products, for example, peroxy radicals, may also be important, as discussed further below with the kinetic model.

DISCUSSION

As mentioned above, we expected that the RH dependence would be mainly driven by the water activity changing with RH leading at first to the following two effects: (i) The increasing water activity and thus increasing volume of the film leads to decreasing volumetric concentrations of CA, P*(t), and $PH^{\bullet}$ and thus of resulting reaction rates. (ii) Water acts as a plasticizer for viscous aqueous organic solutions, leading to decreasing viscosity with increasing water content and thus molecular diffusion coefficients increasing by many orders of magnitude from low to high *RH*.[34] We evaluate the complex interplay of reaction and diffusion with a kinetic model for the overall mechanism shown in Figure 5 to adjust some of the

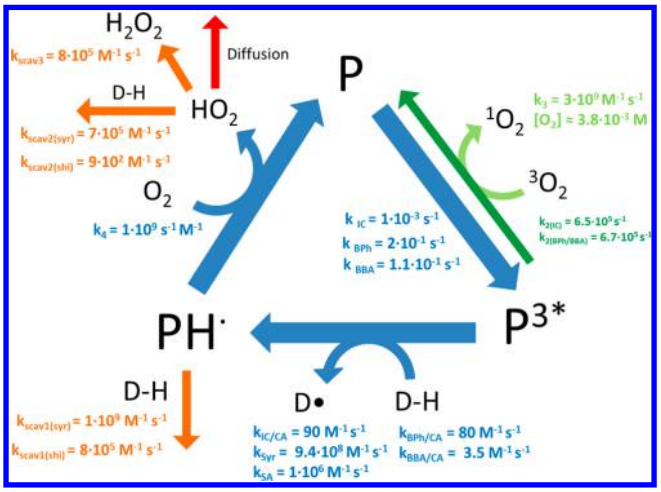

Figure 5. Catalytic mechanism and rate coefficients for the photochemistry of photosensitizers IC, BBA, BPh with a CA and the other H atom donors SA and Syr. Labels for photosensitizer and donors are the same as in Figure 1. Reaction rate coefficients are defined in the SI.

parameters that are not known for the present high solute strength system, to estimate the internal radical turnover and to allow upscaling to atmospheric conditions.

The water activity dependent diffusion coefficient of HO_2 (D_{HO_2}) was first estimated by extrapolating from the data of H_2O diffusion in CA solutions by Lienhard et al.[32,38] (Figure S10, SI). The other parameter values included in Figure 5 were obtained or estimated as described in the SI (Table S2). We first tried to adjust the model to the data of Figure 2 at 55% RH and those for the thickness dependence in Figure S7 with the rate coefficients $k_{IC/CA}$, $k_{BPh/CA}$, $k_{BBA/CA}$, respectively, as the only free variables, because they control $PH^{\bullet}$ production and strongly influence the calculated HO_2 release, as at 55% RH the system was not expected to be under diffusion control. The values estimated in this way for $k_{IC/CA}$, $k_{BPh/CA}$, and $k_{BBA/CA}$ were 90, 80, and 3.5 M^{-1} s^{-1}, respectively. Understandably, they are much lower than for electron rich aromatics in the range 10^5–10^9 M^{-1} s^{-1}.[6,39] There is not enough literature data to compare the relative reactivities among the three sensitizers. The low value for $k_{IC/CA}$ is also consistent with the upper limit obtained from the LFP experiments, $<10^5$ M^{-1} s^{-1}. $k_{IC/CA}$ was then used to calculate the HO_2 release for the RH dependence data (solid line in Figure 3a). Obviously, the calculated HO_2 release exhibits the expected maximum at intermediate RH in Figure 3a, but completely fails in predicting the observed slopes at low and high RH. The sharp falloff of the calculated HO_2 release is due to D_{HO_2} dropping by 6 orders of magnitude between 60% and 20% RH. Related to that, the model also fails to predict the thickness dependence measured at 36% RH. On the other hand the model strongly overpredicts HO_2 release at high RH. We note that solubility of O_2 in organic solvents, such as ethanol, propanol or carboxylic acids, is higher than in water.[40] Thus, O_2 solubility decreases in the transition from a CA rich solution at low RH to a more H_2O rich solution at higher RH (Figure S9). However, the change in O_2 concentration is only about 20%, and due to the significant rate of triplet scavenging by O_2, the lower O_2 concentration increases the triplet concentration with higher water activity and thus compensates the dilution effect. Below 50% RH the decrease in the diffusion controls the decrease of HO_2, and not oxygen solubility, since *D* drops several orders of magnitude down to 0% RH.

The inability of the model to explain the RH dependent reactivity may be related to a dependence of the many rate coefficients on the activity of the reactants (solute strength effects) and also on viscosity. The first suspect was the self-reaction of HO_2, k_{scav3}, motivated by the significant dependence of its gas phase rate coefficient with water vapor pressure.[41] Keeping with the diffusivity as before we parametrized k_{scav3} as a function of RH (see SI) leading to a much lower HO_2 self-reaction rate at lower RH. As a result, the model fits improve with respect to the RH dependence down to around 40% RH (dashed line in Figure 3a) and with respect to the thickness dependence (measured at 36% RH, dashed line in Figure S7). Below 50% RH, diffusion is limiting the HO_2 release, which leads to increasing HO_2 concentration and thus increasing sensitivity to the value of k_{scav3}. At high *RH*, the self-reaction rate is not relevant enough due to fast diffusion of HO_2 out of the film and thus low steady state HO_2 concentrations, so that the change in k_{scav3} does not improve the fit in that range. Also, below 40% RH, the drop of D_{HO_2} dominates the falloff of the modeled HO_2 release.

Motivated by the occurrence of rate limiting surface reactions at low RH in many other multiphase reaction systems,[25,38,42] we added a surface HO_2 production term proportional to the IC concentration adjusted to the thickness dependence in Figure S7 (dashed cyan line). This would provide an explanation for the small offset of the observed linear dependence of the HO_2 release with thickness below 2 μm. The same surface reactivity would then dominate the low RH range in Figure 3a (dashed cyan line). The slight decrease with increasing RH comes from the decrease in IC concentration with increasing water content. Apparently, such a surface process could explain the order of magnitude of HO_2 release at low RH, but in absence of further constraints we refrain from suggesting an explicit RH dependent surface

DOI: 10.1021/acs.est.8b00329
Environ. Sci. Technol. 2018, 52, 7680–7688

reaction model. We also note that such a surface process could also result from phase separation with higher reactivity than expected for a homogeneously mixed system. As an alternative to suggest a surface process and water activity dependence of k_{scav3}, we also evaluated the effect of an alternative parametrization of D_{HO_2}. (Figure S9, dotted line in Figure 3a, dotted line in Figure S7). The results indicate that D_{HO_2} would need to be 4 orders of magnitude higher than that based on the Lienhard et al. data under dry conditions to explain the measured HO_2. In turn, this scenario would be less consistent with the measured thickness dependence of the HO_2 release. In summary, based on the available data and this sensitivity analysis, we are not able to conclusively decide whether the higher than expected HO_2 releases at low RH are due to changes in D_{HO_2}, k_{scav3}, the occurrence of a surface process or a combination thereof.

While we do not assume the medium to affect the initial excitation, ISC may be affected by reduced rotational freedom at high viscosity,[43] leading to increasing ISC yield from low to high RH. There is evidence that hydrogen bonded transition states are involved in electron transfer,[44] proton coupled electron transfer[45] and hydrogen abstraction reactions.[45] This could lead to rates strongly increasing with water activity, not only for k_{scav3}[41] but also for the self-reaction of PH•,[45] their reaction with other organics[46] and the quenching reactions between triplets and organics.[47] As discussed above, while the water activity dependence of k_{scav3} may help to explain the HO_2 release at 30−40% RH, the HO_2 self-reaction is not relevant at high RH. Therefore, the strong drop in HO_2 release between 45% and 65% RH must be the consequence of the water activity dependence of ISC, radical source and radical sink processes, in which the sinks (scavenging reactions of PH• and HO_2) are increasing more strongly with water activity than the sources. In absence of reliable information about solute strength effects on these processes, we refrain from using additional ill-constrained parameters in an attempt to fit to the data. We, therefore, use the parameters valid in the 40−50% RH range for the remainder of the discussion.

For the experiments with Syr and SA shown in Figure 4, all parameters were kept fixed, except k_{SA} and k_{Syr}, to reasonably well reproduce the transition from HO_2 release enhancement by Syr and SA into that of HO_2 scavenging toward higher concentrations. The value of k_{SA} had been adjusted downward from $(2.7 \pm 0.5) \times 10^7$ M^{-1} s^{-1} as determined in the LFP experiments to 1×10^6 M^{-1} s^{-1}. This may be justified by the differences in viscosity for the CWFT (10 Pa s at 40% RH[34]) and the LFP experiments (0.001 Pa s), since electron-transfer reactions may slow down from low to high viscosity.[44] Second, pH in the CWFT and LFP was 1.2 and 7, respectively. Deprotonated acids may undergo 1 order of magnitude faster electron transfer reactions[48] so that k_{SA} measured at pH = 7 likely overestimates the reactivity for the CWFT experiments. In contrast to SA, Syr neither protonates nor deprotonates at pH conditions between the two experiments and thus, values of k_{Syr} are not expected to be affected by the different pH values. Since no reduction in k_{Syr} compared to its values measured by LFP was required to achieve comparable agreement with observations in Figure 4, pH seems to be the dominant factor affecting the reactivity of the IC triplet with Syr and SA under our conditions.

The fate of PH• is the reaction with organics (Syr or SA),[49] self-recombination[46] and reaction with O_2 to produce HO_2. This means that PH• production is fundamental to explain HO_2 production in the condensed phase. This internal radical turnover in the presence of an efficient triplet-state scavenger is substantiated in Figure 6 showing the modeled total

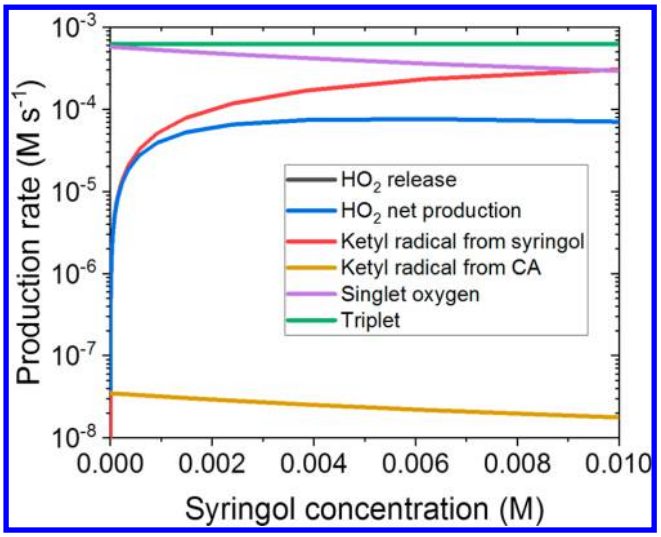

Figure 6. Estimated production of IC ketyl radical, singlet oxygen, IC triplet and HO_2, in the condensed phase film as well as HO_2 release into the gas phase for IC and CA with increasing concentrations of Syr at the same conditions as the CWFT experiments performed with Syr (Figure 4).

production rate of HO_2 in the condensed phase and flux to the gas phase for the conditions of the experiments with Syr presented above at 40% RH. Production of PH• from the reaction with CA and Syr, singlet oxygen and triplet state of IC are also included in Figure 6. The H_2O_2 release to the gas phase predicted by the model is about 10^9 molecules cm^{-2} min^{-1} (10^{-9} M s^{-1}), unfortunately below the detection limit of the H_2O_2 detector used in our experiments.

The internal HO_2 production is predicted to be 3 orders of magnitude greater than its release (dark blue and black lines, respectively, in Figure 6), mostly due to slowed diffusion and the competing scavenging reactions discussed above. The organic radical production is another factor of 10 higher than that of HO_2. Note that as the Syr concentration increases, PH• production increases (red line) while singlet oxygen production decreases (violet line) (Figure 6) implying that radicals, both organic radicals and HO_2, may be preserved and lead to an increasing oxidative capacity within the particle at high organic donor concentration. In the sense of an overall uncertainty estimate, we note that when the ISC is reduced to its lower limit of 0.1, the estimated $k_{IC/CA}$ would have to be increased by a factor of 10 to match with the observations, which would lead to a corresponding reduction of radical production. Even so, with either more reactive donors, or higher concentrations of those similar to Syr, the overall radical production may get comparable.

Upscaling to Atmospheric Conditions. Photochemistry of triplet forming BrC is an important source of radicals in the condensed phase as clearly demonstrated in this study for IC, BBA, and BPh in combination with different oxidation targets. The mass absorption coefficient (MAC) reported by Zhong and Jan[50] for a biomass burning aerosol indicates that roughly 9000 mol of photons per liter of liquid phase of aerosol are absorbed per day assuming 500 nm diameter particles with

DOI: 10.1021/acs.est.8b00329
Environ. Sci. Technol. 2018, 52, 7680−7688

chromophore concentrations of 1 M. This yields an upper limit for triplet production of 900 M day^{-1} considering 0.1 as quantum yield for triplet production.[33] The absorbance of the mixtures used in this study would lead to similar MAC values as those reported by Zhong and Jan.[50] Mass based upper limits of HO_2 release observed in this study were 4.2×10^{16}, 1.4×10^{17}, and 1.4×10^{18} molecule per hour and gram, for IC, BBA, and BPh, respectively. We upscale these fluxes by assuming a suspended aerosol mass of 20 $\mu g\ m^{-3}$, a 12 h irradiation cycle with sinusoidal intensity profile at 0° zenith angle and the ratio of the excitation rates of the photosensitizers from the sun spectrum and that used in our experiments (j_{sun}/j_{lamps} = 2.83, 0.51, and 0.53 for IC, BBA, and BPh, respectively). This leads to an HO_2 release of 2.4×10^{12}, 1.4×10^{12}, and 1.5×10^{13} molecules $m^{-3}\ h^{-1}$ for IC, 4-BBA, and BPh, respectively. These remain far below the full sunlight tropospheric gas phase HO_2 productivity of 10^{17} molecules $m^{-3}\ h^{-1}$.[51] Though, they may become relevant in heavy pollution episodes[8] or when not much light <300 nm driving gas phase radical production is available.

As demonstrated in Figure 6, depending on the presence of more reactive organic oxidation targets (such as electron rich aromatics occurring in biomass burning particles) the total internal radical turnover may exceed the HO_2 release by 4 orders of magnitude. The total condensed phase internal radical production was around up to 10^{17} molecules $m^{-3}\ h^{-1}$. Considering the same assumed aerosol population and light yields an estimated condensed phase HO_2 production of 10^{16} molecule $\mu g^{-1}\ h^{-1}$, which is about 10^{25} molecule $L^{-1}\ h^{-1}$ in the condensed phase or an upper limit of 200 M day^{-1}. For a typical gas phase concentration of 10^6 OH radicals cm^{-3} during the day, its flux into the condensed phase is about 10^{10} molecules $cm^{-2}\ s^{-1}$ or 10^2 molecule s^{-1} into a particle 500 nm in diameter yielding a volume averaged maximum turnover of about 0.2 M day^{-1}. Other radical sources, mainly Fenton chemistry and photolysis of NO_3^- and H_2O_2 contribute about 15 M per day.[52] Therefore, the indirect photochemical radical source addressed here may play an important role in aerosol aging. Clearly, the relative importance of triplet oxidation on aerosol aging may depend on the triplet forming efficiency of real chromophores, size and the microphysical properties of the aerosol particles, and could be clarified by measurements of triplet concentrations in ambient particles.[53]

■ ASSOCIATED CONTENT

Supporting Information

The Supporting Information is available free of charge on the ACS Publications website at DOI: 10.1021/acs.est.8b00329.

Description of the lamps spectrum, solar actinic flux, and absorption spectrum of the compounds used; conversion from NO loss to HO_2 release; details about laser flash photolysis experiments; results from thickness dependence experiments; results from AFT experiments; and details of the kinetic model construction (PDF)

■ AUTHOR INFORMATION

Corresponding Author

*Phone: +41 56 310 4049. E-mail: markus.ammann@psi.ch.

ORCID

Pablo Corral Arroyo: 0000-0003-4090-1623

Thorsten Bartels-Rausch: 0000-0002-7548-2572

Christian George: 0000-0003-1578-7056

Markus Ammann: 0000-0001-5922-9000

Notes

The authors declare no competing financial interest.

■ ACKNOWLEDGMENTS

We would like to thank Laura Gonzalez and Rainer Volkamer for helpful discussions, Mario Birrer for technical support, M.A., P.A., and P.C.A. appreciate support by the Swiss National Science Foundation (Grant 163074). P.A. thanks for funding from the European Union's Horizon 2020 research and innovation program under the Marie Skłodowska-Curie grant agreement No 701647.

■ REFERENCES

(1) Kirchstetter, T. W.; Thatcher, T. L. Contribution of organic carbon to wood smoke particulate matter absorption of solar radiation. *Atmos. Chem. Phys.* **2012**, *12* (14), 6067−6072.

(2) Hoffer, A.; Gelencsér, A.; Guyon, P.; Kiss, G.; Schmid, O.; Frank, G. P.; Artaxo, P.; Andreae, M. O. Optical properties of humic-like substances (HULIS) in biomass-burning aerosols. *Atmos. Chem. Phys.* **2006**, *6* (11), 3563−3570.

(3) Laskin, A.; Laskin, J.; Nizkorodov, S. A. Chemistry of atmospheric brown carbon. *Chem. Rev.* **2015**, *115* (10), 4335−82.

(4) Lee, H. J.; Aiona, P. K.; Laskin, A.; Laskin, J.; Nizkorodov, S. A. Effect of Solar Radiation on the Optical Properties and Molecular Composition of Laboratory Proxies of Atmospheric Brown Carbon. *Environ. Sci. Technol.* **2014**, *48* (17), 10217−10226.

(5) Wong, J. P. S.; Nenes, A.; Weber, R. J. Changes in Light Absorptivity of Molecular Weight Separated Brown Carbon Due to Photolytic Aging. *Environ. Sci. Technol.* **2017**, *51* (15), 8414−8421.

(6) Canonica, S.; Hellrung, B.; Wirz, J. Oxidation of phenols by triplet aromatic ketones in aqueous solution. *J. Phys. Chem. A* **2000**, *104* (6), 1226−1232.

(7) George, C.; Ammann, M.; D'Anna, B.; Donaldson, D. J.; Nizkorodov, S. A. Heterogeneous Photochemistry in the Atmosphere. *Chem. Rev.* **2015**, *115* (10), 4218−4258.

(8) González Palacios, L.; Corral Arroyo, P.; Aregahegn, K. Z.; Steimer, S. S.; Bartels-Rausch, T.; Nozière, B.; George, C.; Ammann, M.; Volkamer, R. Heterogeneous photochemistry of imidazole-2-carboxaldehyde: HO_2 radical formation and aerosol growth. *Atmos. Chem. Phys.* **2016**, *16* (18), 11823−11836.

(9) Yu, L.; Smith, J.; Laskin, A.; Anastasio, C.; Laskin, J.; Zhang, Q. Chemical characterization of SOA formed from aqueous-phase reactions of phenols with the triplet excited state of carbonyl and hydroxyl radical. *Atmos. Chem. Phys.* **2014**, *14* (24), 13801−13816.

(10) Shiraiwa, M.; Yee, L. D.; Schilling, K. A.; Loza, C. L.; Craven, J. S.; Zuend, A.; Ziemann, P. J.; Seinfeld, J. H. Size distribution dynamics reveal particle-phase chemistry in organic aerosol formation. *Proc. Natl. Acad. Sci. U. S. A.* **2013**, *110* (29), 11746−11750.

(11) Herrmann, H.; Ervens, B.; Jacobi, H. W.; Wolke, R.; Nowacki, P.; Zellner, R. CAPRAM2.3: A chemical aqueous phase radical mechanism for tropospheric chemistry. *J. Atmos. Chem.* **2000**, *36* (3), 231−284.

(12) Herrmann, H.; Schaefer, T.; Tilgner, A.; Styler, S. A.; Weller, C.; Teich, M.; Otto, T. Tropospheric Aqueous-Phase Chemistry: Kinetics, Mechanisms, and Its Coupling to a Changing Gas Phase. *Chem. Rev.* **2015**, *115* (10), 4259−4334.

(13) Stemmler, K.; Ammann, M.; Donders, C.; Kleffmann, J.; George, C. Photosensitized reduction of nitrogen dioxide on humic acid as a source of nitrous acid. *Nature* **2006**, *440* (7081), 195−198.

(14) Aregahegn, K. Z.; Nozière, B.; George, C. Organic aerosol formation photo-enhanced by the formation of secondary photosensitizers in aerosols. *Faraday Discuss.* **2013**, *165*, 123.

(15) Kampf, C. J.; Jakob, R.; Hoffmann, T. Identification and characterization of aging products in the glyoxal/ammonium sulfate system; implications for light-absorbing material in atmospheric aerosols. *Atmos. Chem. Phys.* **2012**, *12* (14), 6323−6333.

DOI: 10.1021/acs.est.8b00329
Environ. Sci. Technol. 2018, 52, 7680−7688

(16) Atkinson, R.; Arey, J. Atmospheric Chemistry of Gas-phase Polycyclic Aromatic Hydrocarbons: Formation of Atmospheric Mutagens. *Environ. Health Perspect.* **1994**, *102*, 117−126.
(17) Olariu, R. I.; Barnes, I.; Becker, K. H.; Klotz, B. Rate coefficients for the gas-phase reaction of OH radicals with selected dihydroxybenzenes and benzoquinones. *Int. J. Chem. Kinet.* **2000**, *32* (11), 696−702.
(18) Decesari, S.; Facchini, M. C.; Matta, E.; Mircea, M.; Fuzzi, S.; Chughtai, A. R.; Smith, D. M. Water soluble organic compounds formed by oxidation of soot. *Atmos. Environ.* **2002**, *36* (11), 1827−1832.
(19) Graham, B. Water-soluble organic compounds in biomass burning aerosols over Amazonia1. Characterization by NMR and GC-MS. *J. Geophys. Res.* **2002**, *107* (D20), 8047.
(20) Lienhard, D. M.; Bones, D. L.; Zuend, A.; Krieger, U. K.; Reid, J. P.; Peter, T. Measurements of Thermodynamic and Optical Properties of Selected Aqueous Organic and Organic-Inorganic Mixtures of Atmospheric Relevance. *J. Phys. Chem. A* **2012**, *116* (40), 9954−9968.
(21) Zardini, A. A.; Sjogren, S.; Marcolli, C.; Krieger, U. K.; Gysel, M.; Weingartner, E.; Baltensperger, U.; Peter, T. A combined particle trap/HTDMA hygroscopicity study of mixed inorganic/organic aerosol particles. *Atmos. Chem. Phys.* **2008**, *8* (18), 5589−5601.
(22) Medeiros, P. M.; Simoneit, B. R. T. Source Profiles of Organic Compounds Emitted upon Combustion of Green Vegetation from Temperate Climate Forests. *Environ. Sci. Technol.* **2008**, *42* (22), 8310−8316.
(23) Steimer, S. S.; Lampimäki, M.; Coz, E.; Grzinic, G.; Ammann, M. The influence of physical state on shikimic acid ozonolysis: a case for in situ microspectroscopy. *Atmos. Chem. Phys.* **2014**, *14* (19), 10761−10772.
(24) Steimer, S. S.; Berkemeier, T.; Gilgen, A.; Krieger, U. K.; Peter, T.; Shiraiwa, M.; Ammann, M. Shikimic acid ozonolysis kinetics of the transition from liquid aqueous solution to highly viscous glass. *Phys. Chem. Chem. Phys.* **2015**, *17* (46), 31101−9.
(25) Berkemeier, T.; Steimer, S. S.; Krieger, U. K.; Peter, T.; Pöschl, U.; Ammann, M.; Shiraiwa, M. Ozone uptake on glassy, semi-solid and liquid organic matter and the role of reactive oxygen intermediates in atmospheric aerosol chemistry. *Phys. Chem. Chem. Phys.* **2016**, *18* (18), 12662−74.
(26) Schauer, J. J.; Kleeman, M. J.; Cass, G. R.; Simoneit, B. R. T. Measurement of Emissions from Air Pollution Sources. 3. C1-C29 Organic Compounds from Fireplace Combustion of Wood. *Environ. Sci. Technol.* **2001**, *35* (9), 1716−1728.
(27) Nolte, C. G.; Schauer, J. J.; Cass, G. R.; Simoneit, B. R. T. Highly Polar Organic Compounds Present in Wood Smoke and in the Ambient Atmosphere. *Environ. Sci. Technol.* **2001**, *35*, 1912−1919.
(28) George, C.; Strekowski, R. S.; Kleffmann, J.; Stemmler, K.; Ammann, M. Photoenhanced uptake of gaseous NO_2 on solid organic compounds: a photochemical source of HONO? *Faraday Discuss.* **2005**, *130*, 195.
(29) Ammann, M.; Rössler, E.; Strekowski, R.; George, C. Nitrogen dioxide multiphase chemistry: Uptake kinetics on aqueous solutions containing phenolic compounds. *Phys. Chem. Chem. Phys.* **2005**, *7* (12), 2513−2518.
(30) Atkinson, R.; Baulch, D. L.; Cox, R. A.; Crowley, J. N.; Hampson, R. F.; Hynes, R. G.; Jenkin, M. E.; Rossi, M. J.; Troe, J. Evaluated kinetic and photochemical data for atmospheric chemistry: Volume I - gas phase reactions of O_x, HO_x, NO_x and SO_x species. *Atmos. Chem. Phys.* **2004**, *4*, 1461−1738.
(31) Kurylo, M. J.; Ouellette, P. A.; Laufer, A. H. Measurements of the preassure-dependence of the HO_2 radical self-disproportionation reaction at 298K. *J. Phys. Chem.* **1986**, *90* (3), 437−440.
(32) Lienhard, D. M.; Huisman, A. J.; Bones, D. L.; Te, Y. F.; Luo, B. P.; Krieger, U. K.; Reid, J. P. Retrieving the translational diffusion coefficient of water from experiments on single levitated aerosol droplets. *Phys. Chem. Chem. Phys.* **2014**, *16* (31), 16677−83.
(33) Lamola, A. A.; Hammond, G. S. Mechanisms of Photochemical Reactions in Solution. XXXIII. Intersystem Crossing Efficiencies. *J. Chem. Phys.* **1965**, *43* (6), 2129−2135.
(34) Song, Y. C.; Haddrell, A. E.; Bzdek, B. R.; Reid, J. P.; Bannan, T.; Topping, D. O.; Percival, C.; Cai, C. Measurements and Predictions of Binary Component Aerosol Particle Viscosity. *J. Phys. Chem. A* **2016**, *120* (41), 8123−8137.
(35) Bertram, A. K.; Martin, S. T.; Hanna, S. J.; Smith, M. L.; Bodsworth, A.; Chen, Q.; Kuwata, M.; Liu, A.; You, Y.; Zorn, S. R. Predicting the relative humidities of liquid-liquid phase separation, efflorescence, and deliquescence of mixed particles of ammonium sulfate, organic material, and water using the organic-to-sulfate mass ratio of the particle and the oxygen-to-carbon elemental ratio of the organic component. *Atmos. Chem. Phys.* **2011**, *11* (21), 10995−11006.
(36) Renbaum-Wolff, L.; Song, M.; Marcolli, C.; Zhang, Y.; Liu, P. F.; Grayson, J. W.; Geiger, F. M.; Martin, S. T.; Bertram, A. K. Observations and implications of liquid−liquid phase separation at high relative humidities in secondary organic material produced by alfa-pinene ozonolysis without inorganic salts. *Atmos. Chem. Phys.* **2016**, *16* (12), 7969−7979.
(37) Renbaum-Wolff, L.; Song, M. J.; Marcolli, C.; Zhang, Y.; Liu, P. F. F.; Grayson, J. W.; Geiger, F. M.; Martin, S. T.; Bertram, A. K. Observations and implications of liquid-liquid phase separation at high relative humidities in secondary organic material produced by alpha-pinene ozonolysis without inorganic salts. *Atmos. Chem. Phys.* **2016**, *16* (12), 7969−7979.
(38) Lakey, P. S. J.; Berkemeier, T.; Krapf, M.; Dommen, J.; Steimer, S. S.; Whalley, L. K.; Ingham, T.; Baeza-Romero, M. T.; Pöschl, U.; Shiraiwa, M.; Ammann, M.; Heard, D. E. The effect of viscosity and diffusion on the HO_2 uptake by sucrose and secondary organic aerosol particles. *Atmos. Chem. Phys.* **2016**, *16* (20), 13035−13047.
(39) Jacques, P.; Allonas, X.; Von Raumer, M.; Suppan, P.; Haselbach, E. Quenching of triplet benzophenone by methyl and methoxy benzenes: are triplet exciplexes involved? *J. Photochem. Photobiol., A* **1997**, *111* (1−3), 41−45.
(40) Battino, R.; Rettich, T. R.; Tominaga, T. The Solubility of Oxygen and Ozone in Liquids. *J. Phys. Chem. Ref. Data* **1983**, *12* (2), 163−178.
(41) Kanno, N.; Tonokura, K.; Tezaki, A.; Koshi, M. Water dependence of the HO_2 self reaction: Kinetics of the HO_2-H_2O complex. *J. Phys. Chem. A* **2005**, *109* (14), 3153−3158.
(42) Gržinić, G.; Bartels-Rausch, T.; Berkemeier, T.; Türler, A.; Ammann, M. Viscosity controls humidity dependence of N_2O_5 uptake to citric acid aerosol. *Atmos. Chem. Phys.* **2015**, *15* (23), 13615−13625.
(43) Nagarajan, K.; Mallia, A. R.; Muraleedharan, K.; Hariharan, M. Enhanced intersystem crossing in core-twisted aromatics. *Chem. Sci.* **2017**, *8* (3), 1776−1782.
(44) Ivković-Jensen, M. M.; Kostić, N. M. Effects of viscosity and temperature on the kinetics of the electron-transfer reaction between the triplet state of zinc cytochrome c and cupriplastocyanin. *Biochemistry* **1997**, *36* (26), 8135−8144.
(45) Mitroka, S.; Zimmeck, S.; Troya, D.; Tanko, J. M. How Solvent Modulates Hydroxyl Radical Reactivity in Hydrogen Atom Abstractions. *J. Am. Chem. Soc.* **2010**, *132* (9), 2907−2913.
(46) Tatikolov, A. S.; Sklyarenko, V. I.; Kuzmin, V. A.; Alperovich, M. A. Effect of the solvent on reduction of azomethine dyes with ketyl radicals and recombination of ketyl radicals. *Bull. Acad. Sci. USSR, Div. Chem. Sci.* **1989**, *38* (8), 1597−1601.
(47) Kunze, A.; Muller, U.; Tittes, K.; Fouassier, J. P.; Morlet-Savary, F. Triplet quenching by onium salts in polar and nonpolar solvents. *J. Photochem. Photobiol., A* **1997**, *110* (2), 115−122.
(48) Dave, M. D.; Pande, U. C. Photoinduced electron transfer reaction of 2-mercaptothiazoline and methylene blue: Mechanism and kinetics. *J. Chem. Pharm. Res.* **2012**, *4* (11), 4721−4730.
(49) Rossignol, S.; Aregahegn, K. Z.; Tinel, L.; Fine, L.; Noziere, B.; George, C. Glyoxal Induced Atmospheric Photosensitized Chemistry

DOI: 10.1021/acs.est.8b00329
Environ. Sci. Technol. 2018, 52, 7680−7688

Leading to Organic Aerosol Growth. *Environ. Sci. Technol.* **2014**, *48* (6), 3218−3227.
(50) Zhong, M.; Jang, M. Dynamic light absorption of biomass-burning organic carbon photochemically aged under natural sunlight. *Atmos. Chem. Phys.* **2014**, *14* (3), 1517−1525.
(51) Dusanter, S.; Vimal, D.; Stevens, P. S.; Volkamer, R.; Molina, L. T.; Baker, A.; Meinardi, S.; Blake, D.; Sheehy, P.; Merten, A.; Zhang, R.; Zheng, J.; Fortner, E. C.; Junkermann, W.; Dubey, M.; Rahn, T.; Eichinger, B.; Lewandowski, P.; Prueger, J.; Holder, H. Measurements of OH and HO_2 concentrations during the MCMA-2006 field campaign - Part 2: Model comparison and radical budget. *Atmos. Chem. Phys.* **2009**, *9* (18), 6655−6675.
(52) Tilgner, A.; Bräuer, P.; Wolke, R.; Herrmann, H. Modelling multiphase chemistry in deliquescent aerosols and clouds using CAPRAM3.0i. *J. Atmos. Chem.* **2013**, *70* (3), 221−256.
(53) Kaur, R.; Anastasio, C. First Measurements of Organic Triplet Excited States in Atmospheric Waters. *Environ. Sci. Technol.* **2018**, *52* (9), 5218−5226.

DOI: 10.1021/acs.est.8b00329
Environ. Sci. Technol. 2018, 52, 7680−7688